CCFE-PR(17)66

C J Ham, S C Cowley, G Brochard, and H R Wilson

Nonlinear Ballooning Modes in Tokamaks: Stability and Saturation

Nonlinear Ballooning Modes in Tokamaks: Stability and Saturation

C J Ham[1], S C Cowley[1,2], G Brochard[1,3], and H R Wilson[1,4]

[1]CCFE, Culham Science Centre, Abingdon, Oxon, OX14 3DB
[2]Rudolf Peierls Centre for Theoretical Physics, University of Oxford, Oxford OX1 3NP, UK
[3]Department of Physics, Imperial College, Prince Consort Road, London SW7 2BZ UK
[4]York Plasma Institute, Department of Physics, University of York, Heslington, York YO10 5DD UK

Nonlinear Ballooning Modes in Tokamaks: Stability and Saturation

C J Ham[1], S C Cowley[1,2], G Brochard[1,3], and H R Wilson[1,4]

[1]CCFE, Culham Science Centre, Abingdon, Oxon, OX14 3DB

[2]Rudolf Peierls Centre for Theoretical Physics, University of Oxford, Oxford OX1 3NP, UK

[3]Department of Physics, Imperial College, Prince Consort Road, London SW7 2BZ UK

[4]York Plasma Institute, Department of Physics, University of York, Heslington, York YO10 5DD UK

E-mail: christopher.ham@ukaea.uk

Abstract. The theory of stability and saturation of nonlinear ballooning modes in tokamaks is developed using a generalised Archimedes' principle which is justified for thin elliptical flux tubes. The equation of motion in general geometry is derived and then applied to a simplified 's-α' equilibrium and the nonlinear dynamics of this equilibrium are investigated. This theory shows that the whole pressure and magnetic shear profile is important for nonlinear stability, rather than just the local values which are used for linear stability. The theory shows that for a given pressure profile, nonlinear ballooning saturated states are possible even if the profile is linearly stable to ballooning modes at all radii; the nonlinear ballooning modes are metastable. This occurs particularly at low magnetic shear. The amplitude of the displacement can be as large as the pressure gradient scale length. We conjecture that triggering a transition into these filamentary states can lead to *hard* instability limits. A short survey of different pressure profiles is presented to illustrate the behaviour of the system.

1. Introduction

Ballooning modes are pressure driven instabilities that occur in magnetically confined fusion plasmas and are localized to the bad curvature region [1]. These instabilities can produce both *hard* and *soft* stability limits on the plasma. A *soft* limit is where the plasma pressure gradient is held at a critical value. If the profile goes above this value at any given point the instability is triggered and it produces sufficient transport to drive the pressure profile back to the soft limit value [2]. This may be the process that limits the pressure gradient in the pedestal region of a tokamak plasma. However, there are also *hard* limits which are characterised by an explosive loss of a significant amount of plasma energy. Examples of this are Edge Localized Modes (ELMs) [3], certain types of plasma disruptions in tokamaks, especially discharges with internal transport barriers (ITBs), [4] or the core density collapse in the LHD stellarator [5]. An improved

understanding of what causes a hard limit could lead to strategies to avoid it and thus confidence to run plasmas with steep pressure profiles such as tokamak plasmas with ITBs which could improve the economics of fusion power.

In a series of papers we have shown that the early nonlinear stage of the ballooning mode generates explosively unstable elliptical flux tubes – *"filaments"* [6–8]. The interaction between filaments (flux tubes) tends to suppress the weaker filaments leading to isolated filaments [9]. Thus we have conjectured that the fully nonlinear state of the ballooning type modes is isolated displaced elliptical flux tubes [8]. This conjecture is consistent with observations of (see for example [4, 5, 10]). Recently we investigated the nonlinear states of an elliptical ballooning flux tube in tokamak geometry [11]. In particular, we derived a generalised *Archimedes' principle* [8] and stated the resulting nonlinear equation in toroidal geometry. We will give the full details of the calculation and also survey more of the parameter space in this paper.

In [11] we found that there were ballooning flux tubes which were stable to infinitesimal perturbations but unstable to finite amplitude perturbations. In other words the flux tubes were metastable. Metastability is ubiquitous in the physical sciences but it is largely unexplored in magnetically confined fusion plasmas. For a *hard* instability limit to be possible a finite displaced lower energy state of the plasma must be accessible. In this paper (and in [11]) we examine the possible end states of the ballooning flux tube perturbation – specifically the equilibrium states of the flux tube. In the metastable cases we indeed find lower energy finitely displaced flux tube equilibria. When a metastable plasma approaches the linear stability boundary the energy needed to trigger the nonlinear instability tends to zero. Small amplitude noise in the plasma can trigger onset of the nonlinear instability close to the linear instability boundary. We conjecture that the ballooning mode provides a *hard* instability limit only if there are metastable flux tubes.

In Section 2 we give details of the derivation of the generalised *Archimedes' principle* in general geometry. In Section 3 we calculate the required quantities for the governing equation for a simplified '$s-\alpha$' type equilibrium [12]. Section 4 gives the energy change which results from the flux tube erupting. We examine the case with weak nonlinearity and inertia in Section 5. We discuss the results of a numerical investigation with given pressure gradient and magnetic shear profiles in Section 6. Discussion and Conclusions are given in Section 7. Finally details of our simplified equilibrium calculations are given in Appendix A.

2. Erupting flux tubes in a general axisymmetric equilibrium

In this Section we generalize the treatment of [8] to the geometry of a single isolated flux tube in a general axisymmetric stationary magnetic equilibrium. We shall assume that the flux tube is moving somewhat slower than the sound speed, since we are interested in the behaviour near marginal stability and the saturated states of the flux tube. Consider a field aligned tube of plasma that is displaced through the plasma – sliding along a

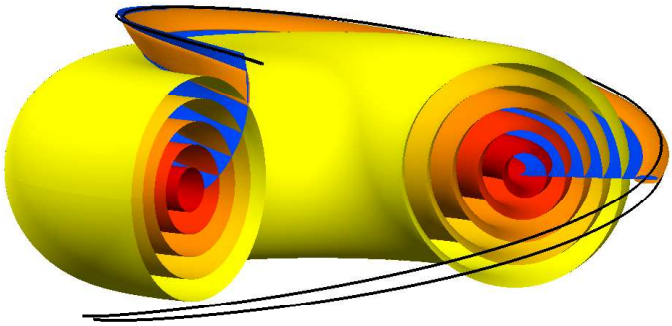

Figure 1: An elliptical (orange) flux tube sliding along the (blue) surface $\mathcal{S} = \mathcal{S}_0$. The external (black) field lines are only slightly perturbed. The tube crosses the (yellow) unperturbed flux surfaces labelled by the variable r. The equations for a field line in the tube which starts on the $r = r_0$ surface is $r = r(r_0, \theta, t)$ and $\mathcal{S} = \mathcal{S}_0$.

surface that is parallel to the undisplaced magnetic field lines outside the tube see Figure 1. The field inside the tube is denoted $\mathbf{B}_{in}$ and the field outside $\mathbf{B}_{out}$. The tube has an elliptical cross section, elongated in the direction of motion and narrower across ($\delta_1 \ll \delta_2$), see Fig. 2. The exact cross sectional shape of the tube is not important here - just that it is narrow enough that the perturbation of the surrounding field is unimportant and that it is considerably elongated in the direction of motion (see discussion in Section 4 of [8]).

As the erupting tube moves it must follow a surface $\mathcal{S}$, which is tangent to both the tube ($\mathbf{B}_{in} \cdot \nabla\mathcal{S} = 0$) and the surrounding field lines ($\mathbf{B}_{out} \cdot \nabla\mathcal{S} = 0$ see Figure 1). We shall assume that the surrounding field is largely unperturbed – *i.e.* $\mathbf{B}_{out} = \mathbf{B}_0$. We can therefore take the surface $\mathcal{S}$ to be a surface of a Clebsch potential of the unperturbed field, i.e $\mathbf{B}_0 = \nabla\psi \times \nabla\mathcal{S}$. We will use the straight line flux coordinates introduced in Greene, Johnson and Weimer [13]. Thus we use r to label flux surfaces, ϕ the toroidal angle and, θ the straight field-line poloidal angle. We deviate slightly from [13] in choosing $\theta = 0$ to be the outer midplane rather than inner midplane for the simplified circular flux surface ('$s - \alpha$') equilibrium of our example. In the notation of [13]:

$$\mathbf{B}_0 = -\bar{B}_0 R_0 f(r) \nabla r \times \nabla\mathcal{S} \quad where \quad \mathcal{S} = \phi - q(r)(\theta - \theta_0(r)). \tag{1}$$

Where $\bar{B}_0$ and R_0 are constants, $q(r)$ is the safety factor and $\theta_0(r)$ is an arbitrary function. The trajectory of a field line in the flux tube that is displaced from the surface r_0 is:

$$r = r(\theta, r_0, t), \qquad and \quad \mathcal{S} = constant \tag{2}$$

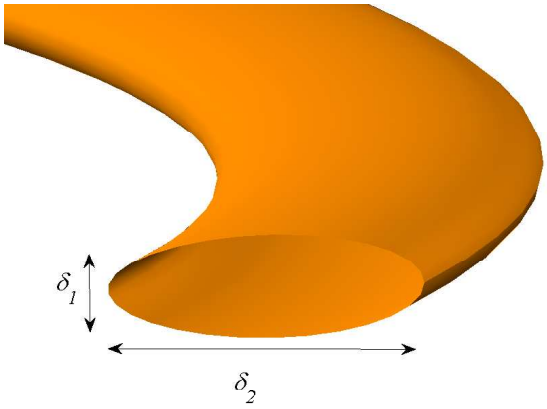

Figure 2: The filament is assumed to be elliptical in shape of width δ_1 in the direction perpendicular the surface $\mathcal{S}$ and δ_2 in the direction of motion along $\mathcal{S}$ with $\delta_2 >> \delta_1$. The fact that the flux tube is elliptical is an assumption, however this is motivated by previous work and physical intuition. First, in linear theory, [1], the eigenfunction across the field is elliptical ($\delta_1 \sim \frac{1}{n}, \delta_2 \sim \frac{1}{\sqrt{n}}$ with $n \gg 1$). Secondly, the weakly nonlinear theory shows that the linear eigenfunction evolves into a narrow elliptical flux tube [6, 7]. Finally, the elliptical shape minimizes sideways distortion of the field to more efficiently extract energy in the fully nonlinear motion.

with the boundary condition $r \to r_0$ as $|\theta| \to \infty$. Note θ measures position along the field line.

The choice of Clebsch potentials is not unique. In principle, we could consider motion along any $\mathcal{S}$ surface defined by any function $\theta_0(r)$. In the '$s-\alpha$' examples given here we restrict ourselves to the choice $\theta_0(r) = 0$. This is the choice for the most linearly unstable motions but not necessarily the most nonlinearly unstable. It is not *a priori* obvious how to choose $\mathcal{S}$, i.e. which Clebsch surface to erupt along. Indeed it is likely to be determined by the dynamics. Our general theory applies to cases where $\theta_0(r) \neq 0$ but we have not explored any specific such cases. The tube wraps around the torus many times and we consider $r(\theta, r_0, t)$ on the domain $-\infty < \theta < \infty$. We ignore the fact that the $\mathcal{S}$ surface intersects itself as θ increases since we assume that the perturbations are sufficiently localised in θ to avoid self intersection of the flux tube. Note this assumption can hold even when the tube localisation in θ is much greater than 2π (as long as r_0 is not a low order rational surface *e.g.* $q(r_0) = 1$). We also assume that flux tubes do not intersect other displaced tubes. The plasma is taken to be perfectly conducting – *i.e.* the plasma is frozen to the field. Thus the field lines must remain attached to their original surfaces and therefore $r = r(\theta, r_0, t) \to r_0$ as $|\theta| \to \infty$. Clearly the surface $\mathcal{S}$ twists, the local twist is a measure of the *local shear* – note the twist of the blue surface in Figure 1. The twist stretches the flux tube making it narrower and longer (Figure 1) as $|\theta|$ increases.

We define the perpendicular vector that is also tangent to the $\mathcal{S}$ surface

$$\mathbf{e}_\perp = \frac{1}{B_0}\boldsymbol{\nabla}\mathcal{S}\times\boldsymbol{B}_0, \tag{3}$$

We define three equilibrium quantities

$$u_\parallel = u_\parallel(r,\theta) = -\bar{B}_0 R_0 f \frac{1}{B_0}\boldsymbol{B}_0\cdot\boldsymbol{\nabla}\theta,$$
$$u_\perp = u_\perp(r,\theta) = \bar{B}_0 R_0 f \frac{1}{B_0}\mathbf{e}_\perp\cdot\boldsymbol{\nabla}\theta, \quad w^2 = w^2(r,\theta) = \frac{u_\parallel^2|\mathbf{e}_\perp|^2}{B_0^2}. \tag{4}$$

Where $|\boldsymbol{B}_0| = B_0$ (not to be confused with the constant $\bar{B}_0$). Since $\mathbf{B}_{in}\cdot\nabla\mathcal{S} = 0$ we must be able to write

$$\mathbf{B}_{in} = B_\parallel(\theta, r_0, t)\mathbf{B}_0 + B_\perp(\theta, r_0, t)\mathbf{e}_\perp \tag{5}$$

The equation for a field line inside the tube is:

$$\left(\frac{\partial r}{\partial\theta}\right)_{r_0,t} = \frac{\mathbf{B}_{in}\cdot\nabla r}{\mathbf{B}_{in}\cdot\nabla\theta} = \frac{B_\perp}{B_\parallel u_\parallel - B_\perp u_\perp} \tag{6}$$

The force (per unit volume) on the plasma is:

$$\mathbf{F} = -\nabla\left[\frac{B^2}{2} + \mu_0 p\right] + \mathbf{B}\cdot\nabla\mathbf{B}. \tag{7}$$

The force across the narrow tube (in the $\nabla\mathcal{S}$ direction) is formally large, $O(p/\delta_1)$, and must cancel to this order, i.e.

$$\mathbf{F}\cdot\nabla\mathcal{S} \sim -|\nabla\mathcal{S}|^2\frac{\partial}{\partial\mathcal{S}}\left[\mu_0 p + \frac{B^2}{2}\right] = 0 \tag{8}$$

Thus integrating across the tube we get:

$$\mu_0 p_{in} + \frac{B_{in}^2}{2} = \mu_0 p_{out} + \frac{B_{out}^2}{2} \tag{9}$$

where 'in' refers to inside the tube and 'out' refers to just outside the tube (at the same r and θ along the tube). We will assume that the field and pressure outside the tube are unperturbed so that:

$$p_{out} = p_0(r) \qquad \text{and} \qquad B_{out} = B_0(r,\theta) \tag{10}$$

are known. The total pressure forces at a point on the tube are thus identical to the pressure forces on the plasma it replaced. We shall assume that the motion of the tube is slow enough that pressure balance along the tube is established – *i.e.* $p_{in} = p(r_0)$. This approximation is obviously correct in the stationary end state of the eruption – a lower energy equilibrium with a finitely displaced tube. Thus

$$B_{in}^2 = B_0^2 + 2\mu_0(p(r) - p(r_0)) \tag{11}$$

Using equation (5) we obtain:

$$B_\parallel^2 = 1 + \frac{2\mu_0(p(r) - p(r_0))}{B_0^2} - B_\perp^2\frac{|\mathbf{e}_\perp|^2}{B_0^2} \tag{12}$$

Thus we obtain expressions for $B_\parallel$ and $B_\perp$

$$B_\parallel = \sqrt{\frac{1+\frac{2\mu_0(p(r)-p(r_0))}{B_0^2}}{\left(1+u_\perp\left(\frac{\partial r}{\partial\theta}\right)_{r_0}\right)^2+w^2\left(\frac{\partial r}{\partial\theta}\right)^2_{r_0}}}\left[1+u_\perp\left(\frac{\partial r}{\partial\theta}\right)_{r_0}\right]$$

$$B_\perp = \sqrt{\frac{1+\frac{2\mu_0(p(r)-p(r_0))}{B_0^2}}{\left(1+u_\perp\left(\frac{\partial r}{\partial\theta}\right)_{r_0}\right)^2+w^2\left(\frac{\partial r}{\partial\theta}\right)^2_{r_0}}}\left[u_\parallel\left(\frac{\partial r}{\partial\theta}\right)_{r_0}\right]. \tag{13}$$

Substituting $r = r(\theta, r_0, t)$ into $p(r)$, $B_0^2(r,\theta)$, $u_\perp(r,\theta)$, $u_\parallel(r,\theta)$ and $w^2(r,\theta)$ in these expressions yields $B_\parallel(\theta, r_0, t)$ and $B_\perp(\theta, r_0, t)$ – *i.e.* along the field line labelled by r_0.

The ideal MHD force, $F_\perp$ pushing the field line along $\mathcal{S}$ in the direction $\mathbf{e}_\perp = (\boldsymbol{\nabla}\mathcal{S}\times\mathbf{B}_0)/B_0$ is:

$$\begin{aligned} F_\perp &= \mathbf{F}\cdot\mathbf{e}_\perp = \frac{1}{\mu_0}\left[\mathbf{B}_{in}\cdot\boldsymbol{\nabla}\mathbf{B}_{in} - \boldsymbol{\nabla}\left(\frac{B_{in}^2}{2}+\mu_0 p_{in}\right)\right]\cdot\mathbf{e}_\perp \\ &= \frac{1}{\mu_0}\left[\mathbf{B}_{in}\cdot\boldsymbol{\nabla}\mathbf{B}_{in} - \mathbf{B}_0\cdot\boldsymbol{\nabla}\mathbf{B}_0\right]\cdot\mathbf{e}_\perp. \end{aligned} \tag{14}$$

The second expression follows from Eq. (9) and the unperturbed equilibrium relation $\boldsymbol{\nabla}\left(B_0^2/2+\mu_0 p_0\right) = \mathbf{B}_0\cdot\boldsymbol{\nabla}\mathbf{B}_0$. Eq. (14) is valid when the tube is sufficiently elliptical that $\delta_1^2 \ll \delta_2^3/\xi$, where ξ is the displacement of the flux tube from its initial position. The expression in Eq. (14) is a generalised form of *Archimedes' principle* where the net force is the curvature force of the tube minus the curvature force of the tube it has displaced.

Substituting equation (5) into (14) we obtain

$$\begin{aligned} F_\perp = {} & (B_\parallel^2-1)(\mathbf{B}_0\cdot\boldsymbol{\nabla}\mathbf{B}_0)\cdot\mathbf{e}_\perp + B_0(B_\parallel\mathbf{B}_0+B_\perp\mathbf{e}_\perp)\cdot\boldsymbol{\nabla}\left(\frac{|\mathbf{e}_\perp|^2}{B_0}B_\perp\right) \\ & - B_\perp^2 B_0^2\mathbf{e}_\perp\cdot\boldsymbol{\nabla}\left(\frac{|\mathbf{e}_\perp|^2}{2B_0^2}\right). \end{aligned} \tag{15}$$

Equation (15) with $B_\parallel$ and $B_\perp$ given by equation (13) determines the force given the shape of the field line, $r(\theta,\psi_0)$ for each r_0. Note that by definition $\mathbf{B}_{in}\cdot\nabla r_0 = (B_\parallel\mathbf{B}_0+B_\perp\mathbf{e}_\perp)\cdot\nabla r_0 = 0$ and therefore $\mathbf{B}_{in}\cdot\nabla \equiv \mathbf{B}_{in}\cdot\nabla\theta\left(\frac{\partial}{\partial\theta}\right)_{r_0}$. Therefore we can treat r_0 as a parameter in equation (15). For an infinitesimal perturbation ($r - r_0 = \xi \ll r_0$) equation (15) reduces to the form familiar from the linear ballooning equation of Connor *et al.* [1]

$$F_\perp \sim B_0\mathbf{B}_0\cdot\nabla\left(\frac{|\mathbf{e}_\perp|^2}{B_0^2}\mathbf{B}_0\cdot\nabla\xi\right) + \frac{2\mu_0}{B_0^3}(\mathbf{e}_\perp\cdot\nabla p)\mathbf{e}_\perp\cdot(\mathbf{B}_0\cdot\boldsymbol{\nabla}\mathbf{B}_0)\xi. \tag{16}$$

The first term in this equation arises from the extra line bending of field lines by the perturbation and is stabilizing. The second term is the change of the field line bending force due to the change of field strength (sometimes called the interchange drive)

The flux tube can have several equilibrium states. Obviously the unperturbed state $r = r_0$, $B_\perp = 0$ and $B_\parallel = 1$ is an equilibrium. We are interested in finding displaced equilibria. Such states of the flux tube must satisfy $F_\perp = 0$ which we write as:

$$(B_\parallel u_\parallel - B_\perp u_\perp)\left(\frac{\partial B_\perp}{\partial \theta}\right)_{r_0} = (B_\parallel^2 - 1)a_1 + B_\perp B_\parallel a_2 + B_\perp^2 a_3 \tag{17}$$

where $u_\perp$ and $u_\parallel$ are defined in equation (4) the coefficients are

$$\begin{aligned} a_1 = a_1(r,\theta) &= \frac{\bar{B}_0 R_0 f \mathbf{e}_\perp \cdot (\mathbf{B}_0 \cdot \nabla \mathbf{B}_0)}{|\mathbf{e}_\perp|^2 B_0} \\ a_2 = a_2(r,\theta) &= \frac{\bar{B}_0 R_0 f \mathbf{B}_0 \cdot \nabla(\frac{|\mathbf{e}_\perp|^2}{B_0})}{|\mathbf{e}_\perp|^2} \\ a_3 = a_3(r,\theta) &= \frac{\bar{B}_0 R_0 f \mathbf{e}_\perp \cdot \nabla(|\mathbf{e}_\perp|^2)}{2|\mathbf{e}_\perp|^2 B_0}. \end{aligned} \tag{18}$$

Equations (17) and (6) with $B_\parallel$ determined from Equation (12) constitute a second order system of one dimensional nonlinear ordinary differential equations for $r = r(\theta, r_0)$ and $B_\perp = B_\perp(\theta, r_0)$ – *i.e.* the equilibrium shape of the displaced field line. As before the equilibria are attained through flux frozen motion so the field lines must stay connected to their original surface. Thus we apply the boundary conditions $r \to r_0$ as $\theta \to \infty$. The tube consists of field lines from a region of r_0 – we can solve for each field line independently. However the calculation of the cross sectional shape of the tube is beyond the scope of this paper.

3. Nonlinear Ballooning Equation in simplified toroidal geometry

We next simplify the nonlinear ballooning equation in general geometry to the large aspect ratio equilibrium with a transport barrier. We calculate the required metrics in a large aspect ratio toroidal geometry with two regions, an outer region where the pressure gradient is small and an narrow (of width $\Delta r \sim \mathcal{O}(\epsilon)$) inner region where the pressure gradient is large, so that we can obtain the nonlinear ballooning equation for this case. We calculate all the elements of the force equation to find a nonlinear generalisation of the '$s - \alpha$' ballooning equation. We need the metric elements from the '$s - \alpha$' large aspect ratio equilibrium. The details of the equilibrium are given in Appendix A.

Using $\mathcal{S} = \phi - q(r)(\theta - \theta_0)$ and metric coefficients from Appendix A.

$$|\mathbf{e}_\perp|^2 = |\boldsymbol{\nabla}\mathcal{S}|^2 = \frac{q^2}{r^2}\left[1 + (s(\theta - \theta_0) - \alpha \sin\theta)^2) + \mathcal{O}(\epsilon)....\right] \tag{19}$$

where $s = rq'/q$ is the magnetic shear and $\alpha = -2\mu_0 R_0 p' q^2/B_0^2$ is the normalised pressure gradient. We have taken $\theta_0 =$ constant since for this simple case we expect that $\theta_0 = 0$. In general we can consider cases with θ_0 a function of r. Using the metric coefficients from the Appendix we obtain:

$$u_\perp = \frac{s(\theta - \theta_0)}{r} + \mathcal{O}(\frac{\epsilon}{r}).... \tag{20}$$

$$u_{\|} = -\frac{\bar{B}_0 r}{q^2 R_0} + \mathcal{O}(\bar{B}_0 \epsilon^2).....\tag{21}$$

$$w^2 = \frac{1}{q^2 R_0^2}\left[1 + (s(\theta-\theta_0) - \alpha\sin\theta)^2) + \mathcal{O}(\epsilon)....\right]\tag{22}$$

The magnetic curvature can be expressed as

$$(\mathbf{B}_0 \cdot \boldsymbol{\nabla}\mathbf{B}_0)\cdot\mathbf{e}_\perp = \mathbf{e}_\perp \cdot \boldsymbol{\nabla}\left(\frac{B_0^2}{2} + p_0(r)\right)$$

$$= \frac{q\bar{B}_0^2}{rR_0}\left[\cos\theta + \sin\theta(s(\theta-\theta_0) - \alpha\sin\theta)\right]\tag{23}$$

The displacement of the flux tube is taken to be of order the transport barrier width so that

$$r - r_0 \sim \mathcal{O}(r\epsilon) \rightarrow \left(\frac{\partial r}{\partial\theta}\right)_{r_0} \sim \mathcal{O}(r\epsilon)\tag{24}$$

which allows the following simplifications

$$B_{\|}^2 - 1 = \frac{2(p_2(r) - p_2(r_0))}{\bar{B}_0^2} \sim \mathcal{O}(\epsilon^2)\tag{25}$$

and

$$B_\perp = -\frac{\bar{B}_0 r}{q^2 R_0}\left(\frac{\partial r}{\partial\theta}\right)_{r_0} \sim \mathcal{O}(\bar{B}_0 r\epsilon^2)\tag{26}$$

$$(\mathbf{B}_{in}\cdot\boldsymbol{\nabla}\theta) = \frac{\bar{B}_0}{qR_0} + \mathcal{O}(\frac{\bar{B}_0\epsilon}{qR_0})\tag{27}$$

We have now calculated all of the elements required for the nonlinear ballooning Eq. (**??**). Substituting them gives the nonlinear ballooning operator in a large aspect ratio tokamak with a transport barrier

$$F_\perp \frac{qR_0^2 r}{\bar{B}_0^2} = (\beta_N(r_0) - \beta_N(r))\left[\cos\theta + \sin\theta(s\theta - \alpha\sin\theta)\right]$$

$$+ \left(\frac{\partial}{\partial\theta}\right)_{r_0}\left(\left[1 + (\alpha\sin\theta - s\theta)^2\right]\left(\frac{\partial r}{\partial\theta}\right)_{r_0}\right)$$

$$- \frac{1}{2}\left(\frac{\partial r}{\partial\theta}\right)_{r_0}^2\left(\frac{\partial}{\partial r}\right)_\theta(\alpha\sin\theta - s\theta)^2\tag{28}$$

where

$$\beta_N(r) = -2R_0 q^2\frac{p_2(r)}{\bar{B}_0^2} \quad\rightarrow\quad \alpha(r) = -\frac{d\beta_N(r)}{dr}\tag{29}$$

Note that in Eq. (28) α is a function of r so that:

$$\left(\frac{\partial\alpha}{\partial\theta}\right)_{r_0} = \left(\frac{\partial r}{\partial\theta}\right)_{r_0}\left(\frac{\partial\alpha}{\partial r}\right)_\theta\tag{30}$$

Our current equation only gives the force. This will allow us to find the saturated states, $F_\perp = 0$, but it does not allow us to look at the time dependent solution of the system. If we assume the time evolution is dominated by viscous drag we can develop a time dependent evolution equation. This is probably too simplistic but it does however allow us the examine the energy evolution. We first need an expression for the velocity, $\mathbf{v} = v\mathbf{e}_\perp$ so that

$$\mathbf{v}\cdot\boldsymbol{\nabla} r = \frac{\partial r}{\partial t} \quad \rightarrow \quad v = -R_0 f \frac{\partial r}{\partial t} \tag{31}$$

We introduce a drag to balance the force $F_\perp = \nu \mathbf{v}\cdot\mathbf{e}_\perp$ (similar to [8]) so that:

$$\begin{aligned}
&\nu'\left(\frac{\partial r}{\partial t}\right)\left[1+(\alpha\sin\theta - s\theta)^2)\right] = \\
&\\
&(\beta_N(r_0)-\beta_N(r))\left[\cos\theta + \sin\theta(s\theta-\alpha\sin\theta)\right] \\
&\\
&+\left(\frac{\partial}{\partial\theta}\right)_{r_0}\left(\left[1+(\alpha\sin\theta-s\theta)^2\right]\left(\frac{\partial r}{\partial\theta}\right)_{r_0}\right) \\
&-\frac{1}{2}\left(\frac{\partial r}{\partial\theta}\right)^2_{r_0}\left(\frac{\partial}{\partial r}\right)_\theta(\alpha\sin\theta-s\theta)^2
\end{aligned} \tag{32}$$

with $\nu' = \nu\frac{q^2R_0^2}{B_0^2}$. This a nonlinear evolution equation for the flux tube position $r(\theta, r_0, t)$. Note that if we linearise Eq. (32) ($r - r_0 \ll \epsilon r$) we recover the usual '$s-\alpha$' equation for ballooning modes.

Figure 2 shows a typical solution of the ballooning mode equation in simplified toroidal geometry. A orange flux tube has ballooned out, moving along the blue surface $\mathcal{S}$=0. This surface is twisted because of the magnetic shear in the system. The flux tube parts the black field lines outside which means that the flux tube can move without reconnection ocuring. The displacement of the flux tube is larger on the low field, or outboard, side. The flux tube is stretched on the inboard side due to the magnetic shear. In figure 2 the trajectory (in θ) of the displaced field lines inside the tube is a solution of the ballooning equation (32) and the distortion of the cross section by magnetic shear is calculated – however the outboard shape of the tubes is guessed.

4. Energy Equation

In [8] we derived an energy (or action) that is stationary for equilibria and minimised for stable equilibria. This is;

$$\begin{aligned}
\mathcal{E} &= \int_{-\infty}^{\infty}\mathbf{B}_{in}\cdot d\mathbf{r} = \int_{-\infty}^{\infty} B_{in}^2\frac{d\theta}{\mathbf{B}_{in}\cdot\boldsymbol{\nabla}\theta} \\
&= \int_{-\infty}^{\infty} B_{in}(r,\theta)\sqrt{1+\frac{r^2|\boldsymbol{\nabla} r|^2}{R_0^2q^2}}\sqrt{\left(1+z\left(\frac{\partial r}{\partial\theta}\right)_{r_0}\right)^2 + w^2\left(\frac{\partial r}{\partial\theta}\right)^2_{r_0}}\,qRd\theta
\end{aligned}$$

where we have used Eq. (22). This integral is performed keeping r_0 constant – *i.e.* we take $r = r(\theta, r_0, t)$. The integral is formally infinite so we should subtract the unperturbed integral – Eq. (33) with $r = r_0$.

Expanding in inverse aspect ratio for our case we obtain the energy/action:

$$\begin{aligned}\mathcal{E} = & \int_{-\infty}^{\infty} d\theta \left[\frac{1}{2}\left(\frac{\partial r}{\partial \theta}\right)_{r_0}^2 \left(1 + (\alpha \sin\theta - s\theta)^2\right)\right] \\ & - \int_{-\infty}^{\infty} d\theta \left[\left(\mathcal{A}(r, r_0)\cos\theta + \mathcal{B}(r, r_0)\theta \sin\theta - \mathcal{C}(r, r_0)(\sin\theta)^2\right)\right] \end{aligned} \tag{33}$$

where the new coefficients are:

$$\begin{aligned}\mathcal{A}(r, r_0) = & \int_{r_0}^{r} (\beta_N(r') - \beta_N(r_0)) dr' \\ \mathcal{B}(r, r_0) = & \int_{r_0}^{r} (\beta_N(r') - \beta_N(r_0)) s(r') dr' \\ \mathcal{C}(r, r_0) = & \frac{1}{2}(\beta_N(r) - \beta_N(r_0))^2 \end{aligned} \tag{34}$$

It is straight forward to show that equilibrium solutions of equation (32) are stationary states under variation of $r = r(\theta, r_0)$ in (33). The evolution of $\mathcal{E}$ using Eq. (32) is

$$\nu' \int_{-\infty}^{\infty} d\theta \left[\left(\frac{\partial r}{\partial t}\right)_{r_0,\theta}^2 \left(1 + (\alpha \sin\theta - s\theta)^2\right)\right] = -\frac{d\mathcal{E}}{dt}. \tag{35}$$

Note that the energy must always decrease in the drag evolution so that it seeks out the minimum energy equilibrium states.

5. Weak Nonlinearity – with Inertia

Here we investigate the weakly nonlinear case including inertia analytically. The dynamics is interesting because the mode spreads along the field lines as it evolves. If we have $r - r_0 \ll \epsilon r$ close to marginal stability, we can expand Eq. (32). Let $x = r - r_0 \sim \mathcal{O}(\delta) \ll 1$ and define the linear operator:

$$\begin{aligned}\mathcal{L}(x) = & \alpha_0 \left[\cos\theta + \sin\theta(s_0\theta - \alpha_0 \sin\theta)\right] x \\ & + \left(\frac{\partial}{\partial \theta}\right)_{r_0} \left(\left[1 + (\alpha_0 \sin\theta - s_0\theta)^2\right] \left(\frac{\partial x}{\partial \theta}\right)_{r_0}\right) \end{aligned} \tag{36}$$

where $s_0 = s(r_0)$ and $\alpha_0 = \alpha(r_0)$. The expanded nonlinear operator is:

$$\mathcal{N}(x, x) = \left[\frac{\alpha_0'}{2}\cos\theta + \theta \sin\theta\left(\frac{\alpha_0' s_0}{2} + s_0'\alpha_0\right) + \frac{3\alpha_0'\alpha_0}{2}\sin^2\theta\right] x^2$$

$$+\left(\frac{\partial}{\partial\theta}\right)_{r_0}\left((\alpha_0'\sin\theta - s_0'\theta)(\alpha_0\sin\theta - s_0\theta)x\left(\frac{\partial x}{\partial\theta}\right)_{r_0}\right)$$

$$-\left(\frac{\partial x}{\partial\theta}\right)^2_{r_0}(\alpha_0'\sin\theta - s_0'\theta)(\alpha_0\sin\theta - s_0\theta) \tag{37}$$

and $s_0' = \frac{ds_0}{dr_0}$ and $\alpha_0' = \frac{d\alpha_0}{dr_0}$. We take the time derivative to be small, specifically $\frac{\partial}{\partial t} \sim \mathcal{O}(\delta)$. The equation of motion, with inertia instead of drag, to the order we need becomes

$$\left(\frac{\partial^2 x}{\partial t^2}\right)\left[1 + (\alpha\sin\theta - s\theta)^2)\right] = \mathcal{L}(x) + \mathcal{N}(x,x) \tag{38}$$

The solution has two regions: an inner region where $\theta \sim \mathcal{O}(1)$ and inertia is unimportant and an outer region where $\theta \sim \mathcal{O}(\delta^{-1})$ and nonlinearity is unimportant. This is similar to the treatment in [7].

5.1. Inner region

In the region $x \sim \mathcal{O}(\delta)$ the left hand side of Eq. (38) is $\sim \mathcal{O}(\delta^3)$. To order δ we have:

$$0 = \mathcal{L}(x) + \mathcal{O}(\delta^2) \tag{39}$$

Then we can write:

$$x(\theta,t) = A(t)x_{Lin}(\theta) + \delta x(\theta,t) \tag{40}$$

where $x_{Lin}(\theta)$ is the linear solution to $\mathcal{L}(x_{Lin}) = 0$ that is even in θ and normalised so that $x_{Lin}(0) = 1$ – thus $A \sim \mathcal{O}(\delta)$. $\delta x(\theta,t) \sim \mathcal{O}(\delta^2)$ is driven by the nonlinear term. As we will see below, the solution as $|\theta| \to \infty$ consists of the "small" and "large" solutions:

$$x_{Lin}(\theta) \to x_{LLin} + \frac{x_{SLin}}{\theta} = x_{SLin}\left(\frac{1}{\theta} + \frac{1}{\Delta'}\right) \tag{41}$$

where x_{SLin} x_{LLin} and $\Delta' = x_{SLin}/x_{LLin}$ are constants. To be consistent we need to be sufficiently close to marginal stability ($\frac{1}{\Delta'} = 0$) such that $\frac{1}{\Delta'} \sim \mathcal{O}(\delta)$. Thus the "large" solution is the same size as $\delta x(\theta,t) \sim \mathcal{O}(\delta^2)$ and we must calculate the corrections due to the nonlinear term to get the correct asymptotic behaviour when $\theta \gg 1$. To order $\mathcal{O}(\delta^2)$ the inner region solution satisfies:

$$0 = \mathcal{L}(x) + A^2\mathcal{N}(x_{Lin}, x_{Lin}) \tag{42}$$

Multiplying Eq. (42)by $x_{Lin}(\theta)$ and integrating from $\theta = 0$ to $\theta = \theta_{match}$ (in the matching region where $1 \ll \theta_{match} \ll \delta^{-1}$) we obtain:

$$s_0^2\theta_{match}^2\left[x(\theta_{match},t)\frac{\partial x_{Lin}}{\partial\theta_{match}} - x_{Lin}(\theta_{match})\frac{\partial x}{\partial\theta_{match}}\right] =$$

$$A^2\int_0^{\theta_{match}} d\theta\left(\left[\frac{\alpha_0'}{2}\cos\theta + \theta\sin\theta(\frac{\alpha_0' s_0}{2} + s_0'\alpha_0) + \frac{3\alpha_0'\alpha_0}{2}\sin^2\theta\right]x_{Lin}^3\right)$$

$$-3A^2\int_0^{\theta_{match}} d\theta x_{Lin}\left(\left(\frac{\partial x_{Lin}}{\partial\theta}\right)_{r_0}^2 2(\alpha_0'\sin\theta - s_0'\theta)(\alpha_0\sin\theta - s_0\theta)\right)$$
$$= c_{NL}A^2. \tag{43}$$

The constant c_{NL} defined by Eq. (43) is $\mathcal{O}(1)$ and insensitive to the choice of θ_{match} as long as it is in the range $1 \ll \theta_{match} \ll \delta^{-1}$ – the particular choice makes a difference to c_{NL} of order δ^2. Since the nonlinear terms in Eq. (42) die away rapidly for asymptotically large θ (see next subsection) we can write:

$$x(\theta_{match}) \to A(t)\frac{x_{SLin}}{\theta_{match}} + x_{Large}(t) \tag{44}$$

Substituting into Eq. (43) we obtain the relation

$$-\frac{x_{Large}(t)}{x_{SLin}} = -\frac{A}{\Delta'} + c_{NL}'A^2. \tag{45}$$

where $c_{NL}' = \frac{c_{NL}}{s_0^2 x_{SLin}^2}$.

5.2. Outer Solution

Now let us expand Eq. (38) in powers of δ with $\frac{\partial}{\partial t} \sim \mathcal{O}(\delta)$, $\theta \sim \mathcal{O}(\delta^{-1})$ and $x \sim \mathcal{O}(\delta^2)$. We treat the θ variation as having two scales: the fast periodic scale $\frac{\partial}{\partial\theta_f} \sim \mathcal{O}(1)$ and the slow scale $\frac{\partial}{\partial\theta_s} \sim \mathcal{O}(\delta)$; then $\frac{\partial}{\partial\theta} = \frac{\partial}{\partial\theta_f} + \frac{\partial}{\partial\theta_s}$ and $\theta_s \sim \mathcal{O}(\delta^{-1})$ – thus $x(\theta_f, \theta_s, t)$. We write $x = x_2 + x_3 + x_4 ....$ where subscript indicates order in δ. To $\mathcal{O}(1)$ we obtain:

$$0 = \theta_s^2\left(\frac{\partial^2 x_2}{\partial\theta_f^2}\right) \quad \to \quad x_2 = x_2(\theta_s, t) \tag{46}$$

In $\mathcal{O}(\delta)$ we obtain:

$$0 = s_0^2\theta_s^2\left(\frac{\partial^2 x_3}{\partial\theta_f^2}\right) + \alpha_0 s_0 \sin\theta_f \theta_s x_2 \quad \to \quad x_3 = x_2\frac{\alpha_0}{s_0}\frac{\sin\theta_f}{\theta_s} \tag{47}$$

In $\mathcal{O}(\delta^{\mathbf{2}})$ we obtain:

$$s_0^2\theta_s^2\left(\frac{\partial^2 x_2}{\partial t^2}\right) = \alpha_0\cos\theta_f x_2 + s_0^2\frac{\partial}{\partial\theta_s}\left(\theta_s^2\frac{\partial x_2}{\partial\theta_s}\right)$$
$$+\frac{\partial}{\partial\theta_f}\left(2s_0^2\theta_s^2\frac{\partial x_3}{\partial\theta_s} - 2\alpha_0 s_0(\sin\theta_f)\theta_s(\frac{\partial x_3}{\partial\theta_f} + \frac{\partial x_2}{\partial\theta_s}) + s_0^2\theta_s^2\frac{\partial x_4}{\partial\theta_f}\right) \tag{48}$$

Note the largest nonlinear term is $\mathcal{O}(\delta^3)$ and is therefore ignored. We average Eq. (48) over the fast scale θ_f to obtain the evolution equation for x_2:

$$\theta_s^2\left(\frac{\partial^2 x_2}{\partial t^2}\right) = \frac{\partial}{\partial\theta_s}\left(\theta_s^2\frac{\partial x_2}{\partial\theta_s}\right) \tag{49}$$

Since x_2 only depends on the one, slow, scale we drop the subscript s on θ and write $x_2 = \frac{f(\theta,t)}{\theta}$. Then Eq. (49) becomes the wave equation:

$$\frac{\partial^2 f}{\partial t^2} = \frac{\partial^2 f}{\partial\theta^2} \tag{50}$$

To satisfy the boundary conditions we take outgoing waves:

$$f(\theta, t) = f(t - \theta). \tag{51}$$

Now we match our solution to the inner solution: The outer solution for $1 \ll \theta \ll \delta^{-1}$ matches Eq. (44), so expanding x_2 for small θ we find:

$$x_2 = \frac{f(t-\theta)}{\theta} \to \frac{f(t)}{\theta} - \frac{df(t)}{dt} = A(t)\frac{x_{SLin}}{\theta} + x_{Large}(t) \tag{52}$$

Thus:

$$f(t) = A(t)x_{SLin} \quad and \quad x_{Large}(t) = -\frac{df(t)}{dt} = -x_{SLin}\frac{dA}{dt} \tag{53}$$

Then Eq. (45) becomes:

$$\frac{dA}{dt} = -\frac{A}{\Delta'} + c'_{NL}A^2. \tag{54}$$

Note this equation is only valid close to the marginal point where $\Delta' \sim \delta^{-1}$. The solution for $A(t=0) = A_0$ is:

$$A(t) = A_0 e^{\gamma t}\frac{1}{1 + cA_0(1 - e^{\gamma t})} \tag{55}$$

where $\gamma = -\Delta'^{-1}$ and $c = c'_{NL}\Delta'$. For linearly damped modes ($\gamma < 0$) If the initial condition $cA_0 > -1$ then as $t \to \infty$ then $A \to 0$. When $cA_0 < -1$ the solution reaches a finite time singularity when $t = (1/\gamma)\ln(1 + \frac{1}{cA_0})$ (see [6]). Clearly the weak nonlinear assumption will be violated before the tube reaches infinite amplitude – a full nonlinear solution is needed in such cases. In ([6]) and ([7]) the weak nonlinear dynamics close to linear marginal stability is treated without the assumption of isolated flux tubes – this is a more complete treatment since it includes the evolution of the flux tube cross section. The explosive nonlinearity (the A^2 term) is present in both treatments.

6. Numerical investigation

The problem described in the previous sections is solved numerically in this section. The problem can be solved as a time dependent drag evolution system or via directly finding the saturated states. We focus on calculating the saturated states in this work. The time dependent method was used in [11].

6.1. Profiles

We investigate the model of a transport barrier type of equilibrium, since we see filamentary structures exploding from such profiles in tokamak experiments, for example, ELMs from the edge transport barrier or ballooning modes from ITBs in TFTR [4]. The model is specified in terms of magnetic shear $s(r)$, and pressure gradient, $\alpha(r)$. The pressure gradient for this model is

$$\alpha = -q^2 R_0 \frac{d\beta_N}{dr} = \alpha_0 \mathrm{sech}^2\left(\frac{r - r_\alpha}{\epsilon}\right). \tag{56}$$

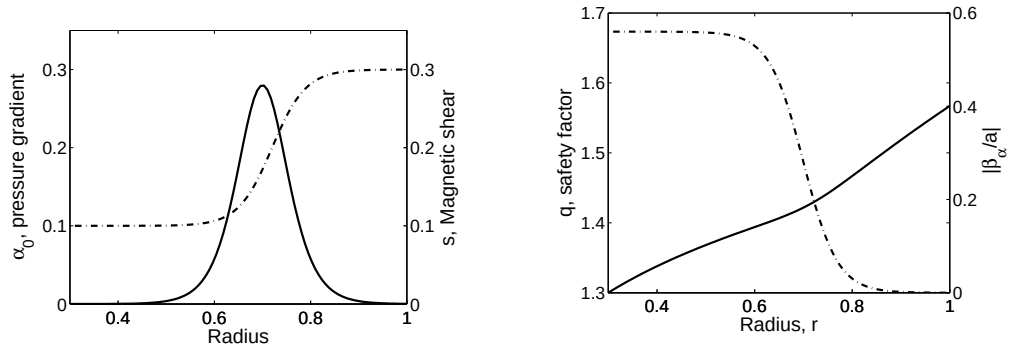

(a) (b)

Figure 3: Transport barrier profiles used in this numerical investigation: a) magnetic shear, $s(r)$, and pressure gradient $\alpha(r)$; and b) safety factor and pressure profiles used for this numerical investigation.

and the shear profile is

$$s(r) = s_0 + \frac{s_1 - s_0}{2}\left(\tanh\left(\frac{r - r_s}{\epsilon}\right) + 1\right). \tag{57}$$

These produce pressure and β profiles

$$p_2(r) = \epsilon p_2\left(1 - \tanh\left(\frac{r - r_\alpha}{\epsilon}\right)\right) \tag{58}$$

which gives a plasma β_N profile

$$\beta_N(r) = -\alpha_0\epsilon\left(1 - \tanh\left(\frac{r - r_\alpha}{\epsilon}\right)\right). \tag{59}$$

In this paper, we will use the following parameters for the base case: $s_0 = 0.1$, $s_1 = 0.3$, $\alpha_0 = 0.28$, $\epsilon = 0.07$, $r_a = 0.7$ and $r_s = 0.72$.

6.2. Time dependent equation

Equation (32) can be solved using an explicit Euler scheme in time and in space. An initial perturbation of the field line is required and we choose

$$r_{init}(\theta) = r_0 + D_0\mathrm{sech}^2\left(\frac{\theta}{\delta_i}\right) \tag{60}$$

where D_0 is the initial amplitude and δ_i gives the width of the initial perturbation.

Formally, the boundary conditions are at $\pm\infty$, so that $r(\pm\infty) \to r_0$; however numerically this need to be truncated. The value of θ where the truncation occurs has been investigated numerically, as has the required time and space steps to get good convergence. Results of this method were shown in [11] and we will not focus on this method here.

6.3. Time independent equation

We can also solve for the time independent states by setting the time derivatives in Eq. (32) to zero and using a shooting method. In some cases we find that the only solution is the stable unperturbed state. Other cases however produce three solutions; one is unstable, and so is not found by the time dependent code, and the other two are stable. One of these stable states represents the saturated filament. If the system is initially linearly stable then the initial field line is one stable state and the unstable state is the critical displacement required for the fieldline to evolve to the other stable state. If the system is linearly unstable then the initial fieldline in unstable and there are two saturated states. Finding the equilibria is considerably faster than the time dependent method and so we focus on it here. Again, we have looked at the convergence with respect to the truncated box length. We have picked a value of the box length such that the results are well converged yet the run takes a reasonable time.

6.4. Evaluation of energy integrals

It is not sufficient that at saturated state is available for a filament to be produced by the plasma. The saturated states must be energetically favourable as well. We therefore need to calculate the change in energy for our profiles to be able to determine if the saturated states are energetically favourable. The integrals in equation (34) can be calculated exactly for the profiles of pressure and shear that we are using by noting that

$$\begin{aligned}\mathcal{A}(r,r_0) &= \int_{r_0}^{r}(\beta_N(r')-\beta_N(r_0))dr' \\ &= \epsilon\alpha_0\left[\epsilon\log\left(\cosh\left(\frac{r'-r_\alpha}{\epsilon}\right)\right)-r'\tanh\left(\frac{r_0-r_\alpha}{\epsilon}\right)\right]_{r_0}^{r} \end{aligned} \tag{61}$$

$$\begin{aligned}\mathcal{B}(r,r_0) &= \int_{r_0}^{r}(\beta_N(r')-\beta_N(r_0))s(r')dr' \\ &= \left(\frac{s_0+s_1}{2}\right)\mathcal{A}(r,r_0)+\epsilon\alpha_0\left(\frac{s_1-s_0}{2}\right)\times \\ &\quad\left[r'+\epsilon\coth\left(\frac{r_\alpha-r_s}{\epsilon}\right)\left[\log\left(\cosh\left(\frac{r'-r_\alpha}{\epsilon}\right)\right)-\log\left(\cosh\left(\frac{r'-r_s}{\epsilon}\right)\right)\right]\right]_{r_0}^{r} \\ &\quad-\left[\epsilon^2\alpha_0\left(\frac{s_1-s_0}{2}\right)\tanh\left(\frac{r_0-r_\alpha}{\epsilon}\right)\log\left(\cosh\left(\frac{r'-r_s}{\epsilon}\right)\right)\right]_{r_0}^{r}\end{aligned} \tag{62}$$

$$\begin{aligned}\mathcal{C}(r,r_0) &= \frac{1}{2}(\beta_N(r)-\beta_N(r_0))^2 \\ &= \frac{\epsilon^2\alpha_0^2}{2}\left(\tanh\left(\frac{r-r_\alpha}{\epsilon}\right)-\tanh\left(\frac{r_0-r_\alpha}{\epsilon}\right)\right)^2\end{aligned} \tag{63}$$

6.5. Stable profiles

First, we show in Fig. 4 four trajectories in '$s - \alpha$' space where the profiles are both linearly stable and have no nonlinear saturated states available. These plots are calculated by first fixing the values of s_0 and s_1, which amounts to specifying the magnetic shear profile. Next we vary the pressure profile until we find the largest α_0 possible without any saturated states available for th profile. If there is no space between the profile and the linear stability boundary then there are no metastable states for that magnetic shear profile. A large space between the profile and the linear stability mean that metastable states are available in that region. These plots therefore give an indication of the boundaries of the region in '$s - \alpha$' space where nonlinear saturated, or metastable, states are available. However, these are not necessarily lower energy states.

The results in Fig. 4 show that there are more metastable states available at lower shear. In Figs. 4 (a) and (b), at high magnetic shear, there is almost no region of metastability while in Figs. 4 (c) and (d) there is a much larger region of metastability. Figure 5 shows profiles with a larger change in shear. Again, there is a larger region of metastability available when magnetic shear is lower.

6.6. Linearly stable profile

Next, we look at a set of profiles which are stable throughout but has states where the erupted flux tube has a lower energy than the initial state. Figures 6, 7 and 8 show three profiles in the region of metastability. Figures 6 has the largest pressure and the profile is close to the linear stability boundary. There is a broad range of saturated states for a range of values of r_0. There is also a region where energy is released, $r_0 = 0.64 - 0.7$, i.e. the saturated states are energetically favourable. The critical amplitude varies with the starting radius, r_0, but for this profile the critical amplitude is small especially near $r_0 = 0.69$. This means that only a small perturbation is required for the filament to reach a saturated state. In Figure 7, we use a lower value of maximum pressure, however the region where there are saturated states available is similar to the case in Figure 6. The critical perturbation to reach these states is larger and the energy released is slightly lower. Finally, Figure 8 uses a yet lower value of α_0. Here the r_{max} values are simlar to the previous cases but the range of r_0 where a metastable states exist is smaller. The critical perturbation required to access these states has also become larger and none of the saturated states have a lower energy state than the initial axisymmetric state.

Note that in these calculations there is a region where lower flux tubes end up in a saturated states further out than flux tubes starting further up, i.e. for two flux tubes where $r_{0,1} < r_{0,2}$, we have $r_{max,1} > r_{max,2}$, i.e. the fluxtubes overtake.

6.7. Linearly unstable profile

Figure 9 shows a case where the profile crosses the marginal linear stability boundary. We see that in the region where the profile is linearly unstable there is no critical

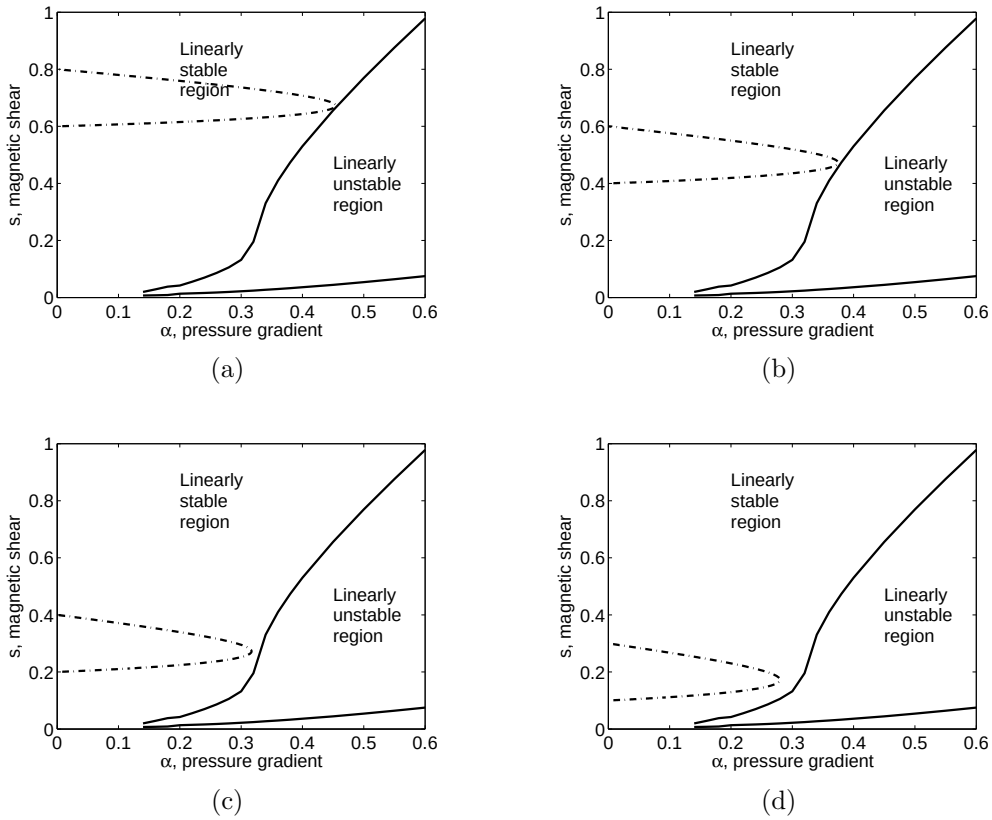

Figure 4: These profiles are all linearly stable and no saturated states are available. The profile starts with the lower value of magnetic shear at the magnetic axis of the plasma and ends at the higher value of shear at the plasma edge. These plots are calculated by fixing the values of s_0 and s_1 and then varying α_0 to find the highest value where the profile has no saturated states. The region between the profile, dashed line, and the ballooning stability boundary, solid line, indicates the region where nonlinear saturated states are available. The values of shear profiles for each plot are: (a) $s_0 = 0.6$, $s_1 = 0.8$; (b) $s_0 = 0.4$, $s_1 = 0.6$; (c) $s_0 = 0.2$, $s_1 = 0.4$; and (d) $s_0 = 0.1$, $s_1 = 0.3$.

perturbation required for a saturated state to exist. There is a broader range of values of r_0 where saturated states exist and the energy released from them is greater than the linearly stable cases. For linearly unstable field lines there is a saturated state that moves outwards and one that moves inwards. The energy change of the outward saturated state is significantly higher (by several orders of magnitude) than the energy of the one that moves inwards, although both have a lower energy level than the initial state. This means they are both energetically favourable as would be expected as a result of linear instability. On the far right of the plot we see that there a a very small region where fieldlines moving inward have a critical perturbation, i.e. these fieldlines are linearly stable.

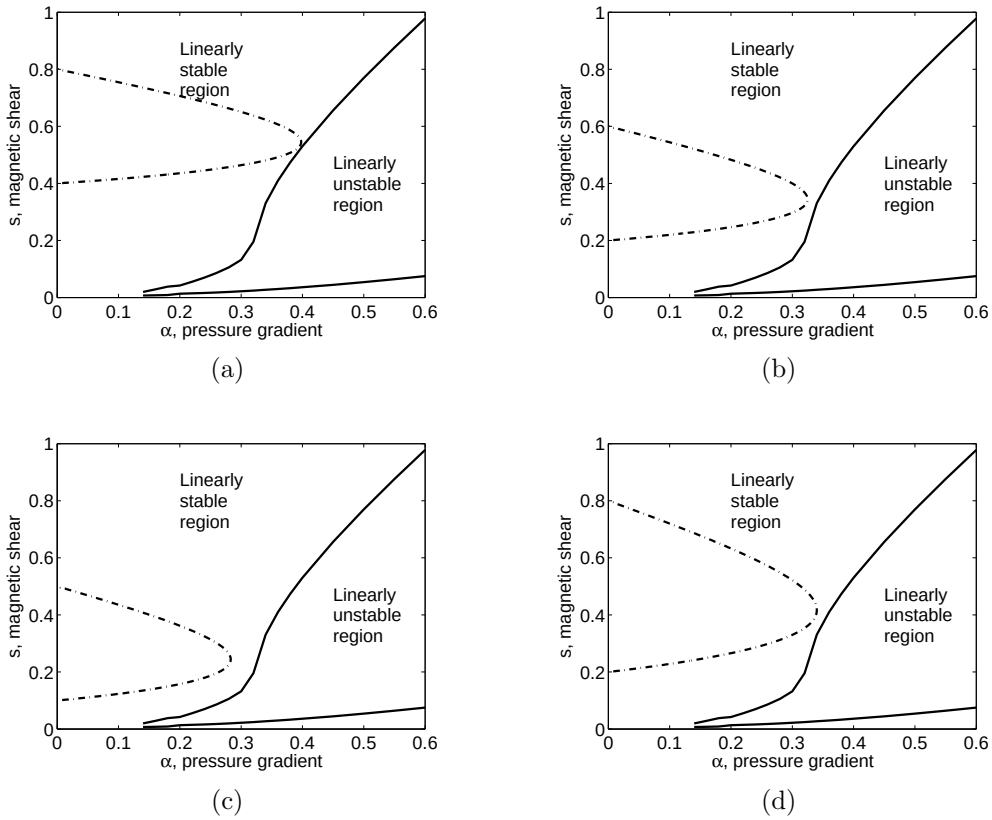

Figure 5: As for Figure 4. The values of shear profiles for each plot are: (a) $s_0 = 0.4$, $s_1 = 0.8$; (b) $s_0 = 0.2$, $s_1 = 0.6$; (c) $s_0 = 0.1$, $s_1 = 0.5$; and (d) $s_0 = 0.2$, $s_1 = 0.8$.

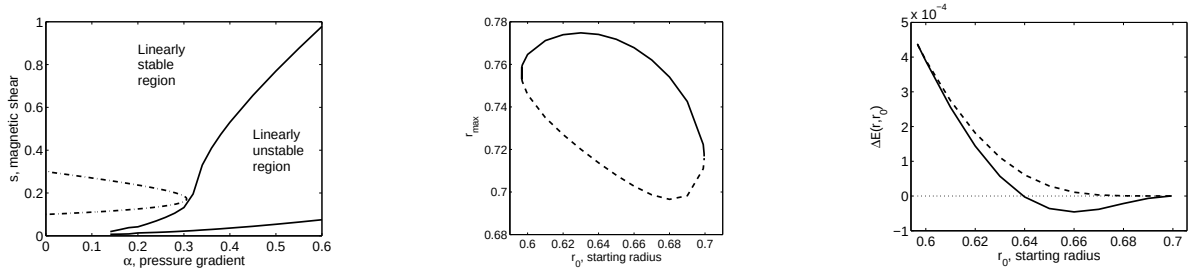

Figure 6: Plot of: (a) trajectory of the profile in '$s - \alpha$' space; (b) plot of the location of the maximum of the saturated state against starting flux surface; (c) the energy change of the saturated state compared to the initial position. Here the trajectory approaches the linear ballooning boundary. A region of lower energy saturated states is available for starting locations from $r_0 = 0.64$ to $r_0 = 0.7$.

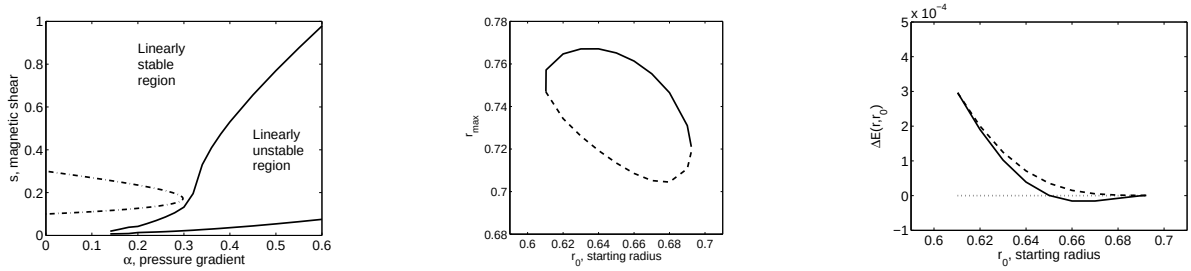

(a) (b) (c)

Figure 7: Plot of: (a) trajectory of the profile in '$s - \alpha$' space; (b) plot of the location of the maximum of the saturated state against starting flux surface; (c) the energy change of the saturated state compared to the initial position. Here the trajectory is further from the linear ballooning boundary. A region of lower energy saturated states is available for starting locations from $r_0 = 0.65$ to $r_0 = 0.69$.

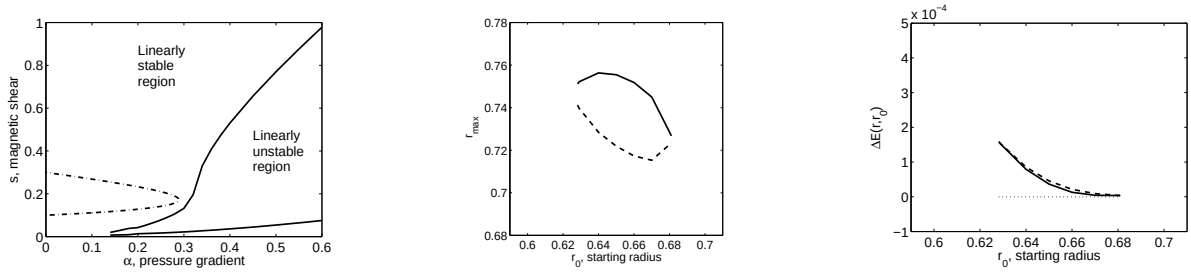

(a) (b) (c)

Figure 8: Plot of: (a) trajectory of the profile in '$s - \alpha$' space; (b) plot of the location of the maximum of the saturated state against starting flux surface; (c) the energy change of the saturated state compared to the initial position. Here the trajectory is further still from the linear ballooning boundary. There is no region where the saturated states have lower energy.

7. Discussion and Conclusions

7.1. Discussion

There is plenty of evidence that filament states exist in experiments, for example ELMs are ubiquitous in tokamak H-mode plasmas and in [11] we discussed the results of Fredrickson [4] which describe a ballooning mode linked with the disruption of internal transport barrier shots. More recently core plasma limits have been observed at LHD [5]. These maybe driven by a three dimensional version of the theory presented here. KSTAR [20] has looked at ELM filament dynamics in more detail experimentally using an ECEI diagnostic. That work shows the emergence of filament structures at the edge of the plasma that saturate and persist for a period of time before the final ELM crash occurs. This at least has qualatative similarity to the saturation phase of the model

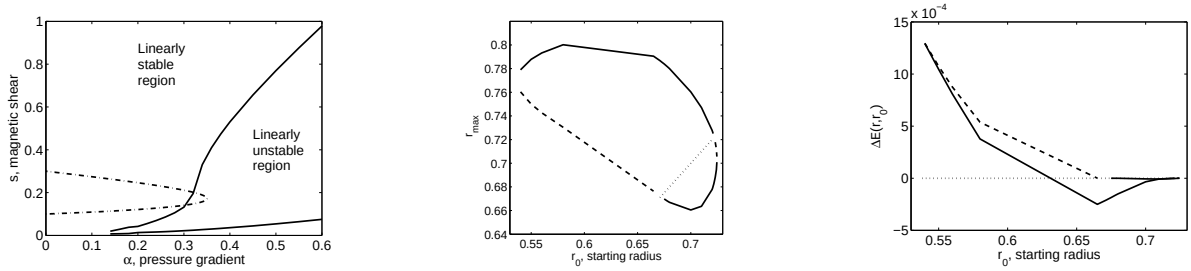

(a) (b) (c)

Figure 9: Plot of: (a) trajectory of the profile in '$s - \alpha$' space; (b) plot of the location of the maximum of the saturated state against starting flux surface (solid line shows the saturated state, dashed line the critical state and dotted line the linearly unstable fieldlines—); (c) the energy change of the saturated state compared to the initial position. The trajectory crosses the linear ballooning boundary and so part of the plasma is linearly unstable.

presented here. We hope to investigate these experimental cases more quantitatively in future work.

It is likely that transport profiles in transport barriers are limited by some soft limit such as the kinetic ballooning mode (KBM). If this is the case then the profile will sit near the linear ballooning stability boundary. This will mean that a small finite perturbation resulting from noise in the plasma could excite a filament to erupt. The model predicts that the profile could be linearly stable throughout the filament production process or at least at the marginal stability boundary. This qualitatively agrees with some analyses of ELMing profiles.

Numerical simulations have investigated the eruption of flux tubes, for example [21, 22] where a nonlinear plasma model examined a 2/1 mode in a hybrid scenario and demonstrated that explosive filament growth was possible. Myers *et al* [23] used an ideal MHD model to look at a slab version of the model presented here. They found a time where the simulation first settled down to the linear eigenmode shape, then a linear growth phase followed by a nonlinear growth, and finally an explosive final phase. It is likely that the explosive phase was under resolved and an extended physics model would almost certainly be necessary in this phase.

There are some assumptions and approximations made in the present model such as the large aspect ratio equilibrium and the elliptical shape of the filaments. The large aspect ratio assumption can be relaxed and the metric quantities calculated in Appendix A can instead be taken from a numerical equilibrium code. Indeed this work is underway. The assumption of the elliptical filaments is more fundamental but is justified by the quasilinear calculations of the expected mode structure [7] and by the results from numerical investigations [21–23]. The elliptical shape can also be justified from physical intuition. It is energetically favourable for the erupting flux tube to perturb the ambient field as little as possible and this is achieved with an elliptic flux tube.

If we accept that these satuated filament states exist, then it will be important to understand the next steps in the dynamics. It may be that the field lines in the flux tube reconnect with the ambient magnetic field at some location, but it is not obvious where this location is. It maybe that there is significant cross field transport out of the ballooned filament, given there will be a strong temperature gradient as suggested in the 'Leaky hosepipe' model [24]. These issues will be addressed in future work.

7.2. Conclusions

The results shown here exhibit a rich dynamics. The key result is that linearly stable flux tubes can erupt to saturated ballooning states, i.e. they are metastable. The experimental transport barrier profiles are likely to sit near the ballooning mode marginal stability boundary and so these modes are likely to appear if a critical perturbation is available. We conjecture that *hard* stability limits arise when the plasma is in a metastable state with a large energy difference between the unperturbed and perturbed equilibria. The closer the profile is to marginal stability, the larger the region of the plasma that has saturated states available and the more favourable the energy change associated with the saturated states. The current model uses a large aspect ratio '$s-\alpha$' model equilibrium but we fully expect that the key qualitative results will also appear when we use realistic experimental geometry in future work. The model may be able to explain key elements of ITB distruption and ELM dynamics when applied to realistic geometry.

Acknowledgements

The authors would like to thank J W Connor and S Pamela for useful discussions. This work has been carried out within the framework of the EUROfusion Consortium and has received funding from the Euratom research and training programme 2014-2018 under grant agreement No 633053 and from the RCUK Energy Programme [grant number EP/P012450/1]. To obtain further information on the data and models underlying this paper please contact PublicationsManager@ukaea.uk. The views and opinions expressed herein do not necessarily reflect those of the European Commission.

Appendix A. Model equilibrium

In these notes we calculate the large aspect ratio ($\epsilon = r/R \ll 1$) equilibrium with two regions; an *Outer Region* where the pressure gradient is small ($rp'/B^2 \sim \mathcal{O}(\epsilon^2)$) and a narrow ($\Delta r \sim \epsilon r$) *Transport Barrier* around $r = r_{TB}$ where the pressure gradient is close to the ballooning threshold ($rp'/B^2 \sim \mathcal{O}(\epsilon)$). Note that the plasma beta is everywhere small *i.e.* $p/B^2 \sim \mathcal{O}(\epsilon^2)$. We shall take the safety factor, q, and the global magnetic shear, rq', to be finite in the transport barrier – however r^2q'' can be large in the transport barrier. All symbols have their usual meaning!

Appendix A.1. Inverse Equilibrium

We use the usual inverse equilibrium approach of Weimer, Greene and Johnson. The radial variable r labels flux surfaces, θ is a poloidal angle and ϕ is the usual cylindrical toroidal angle. In axisymmetry the cylindrical coordinates $(R,\ \phi,\ Z)$ are functions of the flux coordinates $(r,\ \theta)$ – *i.e.* $R = R(r,\theta)$ and $Z = Z(r,\theta)$.

The magnetic field is given by:

$$\mathbf{B} = \bar{B}_0 R_0 \{ f(r) \boldsymbol{\nabla}\phi \times \boldsymbol{\nabla} r + g(r) \boldsymbol{\nabla}\phi \} \tag{A.1}$$

where $\bar{B}_0$ is a normalising field so that $g \sim \mathcal{O}(1)$ and R_0 is the radius of the magnetic axis. The equilibrium Grad-Shafranov equation in flux coordinates is:

$$\frac{1}{r}\frac{\partial}{\partial r}(rf|\nabla r|^2) + f\frac{\partial}{\partial \theta}(\nabla r \cdot \nabla\theta) + \frac{1}{f}(gg' + \frac{R^2}{R_0^2 B_0^2}p') = 0. \tag{A.2}$$

The jacobian of the transformation to the flux coordinates $(r,\ \theta,\ \phi)$ is chosen to keep the field lines *straight* in $\theta - \phi$ space on a flux surface:

$$\mathcal{J} = (\boldsymbol{\nabla} r \times \boldsymbol{\nabla}\theta \cdot \boldsymbol{\nabla}\phi)^{-1} = \frac{rR^2}{R_0} = R\left(\frac{\partial R}{\partial \theta}\frac{\partial Z}{\partial r} - \frac{\partial R}{\partial r}\frac{\partial Z}{\partial \theta}\right) \tag{A.3}$$

and then the safety factor is $q(r) = \frac{rg}{R_0 f}$. Note that:

$$(\boldsymbol{\nabla} r \times \boldsymbol{\nabla}\theta) = \frac{R_0}{r}\boldsymbol{\nabla}\phi \tag{A.4}$$

We expand R and Z as:

$$\begin{aligned} R &= R_0 + r\cos\theta + \tilde{R}_1(r)\cos 2\theta + \bar{R}_1(r) + \mathcal{O}(\epsilon^2 r)..... \\ Z &= -r\sin\theta + \tilde{Z}_1(r)\sin 2\theta + \mathcal{O}(\epsilon^2 r)..... \end{aligned} \tag{A.5}$$

where $\tilde{R}_1$, $\bar{R}_1$ and $\tilde{Z}_1$ are $\mathcal{O}(\epsilon r)$. We have chosen $\theta = 0$ to be the outer (larger R) mid-plane of each flux surface – this differs from the choice in [13] where $\theta = 0$ is on the inner R mid-plane. We define $\bar{B}_0$ so that:

$$g = 1 + g_2 + \mathcal{O}(\epsilon^3), \quad g_2 \sim \mathcal{O}(\epsilon^2) \tag{A.6}$$

and q is finite so that $f = f_1 = \frac{r}{R_0 q} + \mathcal{O}(\epsilon^2)$. To denote order we write $p(r) = p_2(r)$.

We seek expanded expressions as functions of r and θ of the metric elements:

$$\begin{aligned} |\nabla r|^2 &= \frac{R_0^2}{r^2 R^2}\left[\left(\frac{\partial R}{\partial \theta}\right)^2 + \left(\frac{\partial Z}{\partial \theta}\right)^2\right] \\ \nabla r \cdot \nabla\theta &= -\frac{R_0^2}{r^2 R^2}\left[\frac{\partial R}{\partial \theta}\frac{\partial R}{\partial r} + \frac{\partial Z}{\partial r}\frac{\partial Z}{\partial \theta}\right] \\ |\nabla\theta|^2 &= \frac{R_0^2}{r^2 R^2}\left[\left(\frac{\partial R}{\partial r}\right)^2 + \left(\frac{\partial Z}{\partial r}\right)^2\right] \end{aligned} \tag{A.7}$$

to substitute into the ballooning equations of Section (**??**)

The regions are:

Outer Region where $|r - r_{TB}| \gg \epsilon r$ and all radial derivatives are finite *i.e.*

$$\frac{\partial}{\partial r} \sim \mathcal{O}(\frac{1}{r}), \;\; \frac{\partial \tilde{R}_1}{\partial r}, \; \frac{\partial \tilde{Z}_1}{\partial r}, \; \frac{\partial \bar{R}_1}{\partial r} \sim \mathcal{O}(\epsilon), \tag{A.8}$$

$$rp'/B_0^2 \sim \mathcal{O}(\epsilon^2), \quad rg_2' \sim \mathcal{O}(\epsilon^2) \;\; and \;\; f, rf' \sim \mathcal{O}(\epsilon)$$

Transport Barrier where $|r - r_{TB}| \sim \epsilon r$ and radial derivatives are large:

$$\frac{\partial}{\partial r} \sim \mathcal{O}(\frac{1}{\epsilon r}), \;\; \frac{\partial \tilde{R}_1}{\partial r}, \; \frac{\partial \tilde{Z}_1}{\partial r}, \; \frac{\partial \bar{R}_1}{\partial r} \sim \mathcal{O}(\frac{1}{\epsilon}), \tag{A.9}$$

$$rp'/B_0^2 \sim \mathcal{O}(\epsilon), \quad rg_2' \sim \mathcal{O}(\epsilon) \;\; and \;\; f, rf' \sim \mathcal{O}(\epsilon) \;\; but \;\; r^2 f'', r^2 g'' \sim \mathcal{O}(1)$$

Appendix A.2. Outer Region

Substituting expressions from Eq. (A.5) into Eq. (A.3) we obtain:

$$\frac{r^2 \cos\theta}{R_0} = 2\tilde{R}_1 \sin\theta \sin 2\theta - 2\tilde{Z}_1 \cos\theta \cos 2\theta - r \sin\theta \sin 2\theta \frac{\partial \tilde{Z}_1}{\partial r}$$
$$+ r \cos\theta \cos 2\theta \frac{\partial \tilde{R}_1}{\partial r} + r \cos\theta \frac{\partial \bar{R}_1}{\partial r} + \mathcal{O}(r\epsilon^2) \tag{A.10}$$

which yields:

$$\tilde{Z}_1 = -\tilde{R}_1$$

$$r\frac{\partial \bar{R}_1}{\partial r} = \frac{r^2}{R_0} - 2\tilde{R}_1 - r\frac{\partial \tilde{R}_1}{\partial r} \tag{A.11}$$

From Eq. (A.7) we define Δ' so that:

$$|\nabla r|^2 = 1 + 2\Delta' \cos\theta .....$$

$$\rightarrow \tilde{R}_1 = \frac{r^2}{2R_0} + \frac{r\Delta'}{2}$$

$$\bar{R}_1 = \frac{r^2}{2R_0} - \frac{r\Delta'}{2} - \Delta \tag{A.12}$$

and

$$\nabla r \cdot \nabla \theta = -\frac{1}{r}\left(r\Delta'' + \Delta' + \frac{r}{R_0}\right)\sin\theta. \tag{A.13}$$

We will need:

$$\frac{R^2}{R_0^2} = 1 + \frac{2r}{R_0}\cos\theta - \left[\frac{r^2}{2R_0^2} + \frac{2\Delta}{R_0} + \frac{r\Delta'}{R_0}\right] + \left[\frac{r\Delta'}{R_0} + \frac{3r^2}{2R_0^2}\right]\cos 2\theta. \tag{A.14}$$

and

$$|\nabla\theta|^2 = \frac{1}{r^2}\left[1 + 2(\frac{r}{R_0} - \Delta')\cos\theta + (r\Delta'' \sin\theta)^2 .... \mathcal{O}(\epsilon^2)\right] \tag{A.15}$$

We have kept the terms that become large in the transport barrier – where $r\Delta'' \sim 1$. The equilibrium relation, Eq. (A.2), becomes to $\mathcal{O}(\epsilon^2)$:

$$\frac{1}{r}\frac{d}{dr}(rf_1) + \frac{1}{f_1}\left[g_2' + \frac{p_2'}{\bar{B}_0^2}\right] = 0 \tag{A.16}$$

$$\Delta'' = \frac{1}{R_0} - \frac{2R_0q^2}{r}\frac{p_2'}{\bar{B}_0^2} - \left[\frac{3}{r} - 2\frac{2}{q}\frac{dq}{dr}\right]\Delta' \tag{A.17}$$

Appendix A.3. Transport barrier

The equations derived in the previous section, Eqs. (A.12) - (A.17), remain valid to the order we need. Since q and r are roughly constant across the Transport barrier we can integrate Eq. (A.16) for g_2' and Eq. (A.17) for Δ' in the layer.

$$g_2 = -\frac{p_2}{\bar{B}_0^2} + constant \tag{A.18}$$

$$\Delta'' \sim -\frac{2R_0q^2}{r}\frac{p_2'}{\bar{B}_0^2} \sim \mathcal{O}(\frac{1}{r}) \quad \rightarrow \quad \Delta' = -\frac{2R_0q^2}{r}\frac{p_2}{\bar{B}_0^2} + constant \tag{A.19}$$

Note the constants are slowly varying functions of r so they are effectively constant across the transport barrier. The magnetic shear is taken to be finite and finitely varying across the barrier, so that:

$$\begin{aligned} f_1 &= f_1(r) + f_2(\frac{r-r_0}{\epsilon}) \\ q' &= \frac{d}{dr}\left(\frac{R_0f_1}{r}\right) + \frac{R_0f_2'}{r}... \end{aligned} \tag{A.20}$$

We introduce the s and α parameters of Connor, Hastie, Taylor [1]:

$$\begin{aligned} s &= \frac{rq'}{q} \\ \alpha &= -2R_0q^2\frac{p_2'}{\bar{B}_0^2} \end{aligned} \tag{A.21}$$

Note that both these parameters are finite and vary finitely over the transport barrier so that $s' \sim \mathcal{O}(\frac{1}{\epsilon})$ and $\alpha' \sim \mathcal{O}(\frac{1}{\epsilon})$. Then $\Delta'' = \frac{\alpha}{r}$. To lowest (finite) order the metric coefficients are

$$|\nabla r|^2 = 1$$

$$\nabla r \cdot \nabla\theta = \left(\frac{2R_0q^2}{r}\frac{p_2'}{\bar{B}_0^2}\right)\sin\theta = -\frac{\alpha}{r}\sin\theta \tag{A.22}$$

$$|\nabla\theta|^2 = \frac{1}{r^2}\left[1 + (2R_0q^2\frac{p_2'}{\bar{B}_0^2}\sin\theta)^2....\mathcal{O}(\epsilon)\right] = \frac{1}{r^2}\left[1 + (\alpha\sin\theta)^2....\mathcal{O}(\epsilon)\right]$$

We shall also need the derivatives of R.

$$\frac{\partial R}{\partial r} = \cos\theta - \alpha \sin^2\theta + \mathcal{O}(\epsilon)....$$

$$\frac{\partial R}{\partial \theta} = -r\sin\theta + \mathcal{O}(\epsilon).... \tag{A.23}$$

References

[1] J. W. Connor, R. J. Hastie and J. B. Taylor, Proc. R. Soc. London **A365** (1979)
[2] J. W. Connor, J. B. Taylor, and M. Turner, Nucl. Fusion **24** 642(1984)
[3] J. W. Connor *Plasma Phys. Control. Fusion* **40** 531 (1998)
[4] E. D. Fredrickson, et. al. *Phys. Plasmas* **3** 2620 (1996)
[5] S. Ohdachi, et al. *Nucl. Fusion* **57** 066042 (2017)
[6] S. C. Cowley and M. Artun, *Physics Reports,* vol. 283, pp. 185 – 211, 1997.
[7] H. R. Wilson and S. C. Cowley, *Phys. Rev. Lett.*, vol. 92, no. 17, 175006-1– 175006-4, 2004.
[8] S. C. Cowley, B. Cowley, S. A. Henneberg and H. R. Wilson, Proc. R. Soc. A **471** 20140913(2015)
[9] S. A. Henneberg, S. C. Cowley and H. R. Wilson *Plasma Phys. Control. Fusion* **57** 125010 (2015)
[10] A. Kirk , et. al., Phys. Rev. Lett. **96** 185001 (2006)
[11] C J Ham, S C Cowley, G Brouchard and H R Wilson *Phys. Rev. Lett.* **116** 235001 (2016)
[12] J. W. Connor, R. J. Hastie and J. B. Taylor, Phys. Rev. Lett. **40** 396(1978)
[13] J. M. Greene, J. L. Johnson and K. E. Weimer, Phys. Fluids. **14** 671 (1971)
[14] T.C. Hender, et. al. Nucl. Fusion, **47**, S128 - S202(2007).
[15] H. R. Wilson, S. C. Cowley, A. Kirk and P. B. Snyder *Plasma Phys. Control. Fusion* **48** A71-A84 (2006)
[16] P. B. Snyder, et. al., Nucl. Fusion, **51**, 103016 (2011).
[17] J. W. Connor, et. al., Phys. Fluids. **31** 577(1988)
[18] S. C. Cowley, B. Cowley, S. A. Henneberg and H. R. Wilson, arXiv preprint arXiv:1411.7797 (2014),
[19] H. R. Struass *Phys. Fluids* **24** 2004 (1981)
[20] G. S. Yun, et al. *Phys. Rev. Lett.*, vol. 107, 045004, 2011.
[21] A. Y. Aydemir, et al. *Nucl. Fusion* **56** 054001 (2016)
[22] A. Y. Aydemir, et al. *Nucl. Fusion* **58** 016026 (2018)
[23] S. A. Myers, et al. *Plasma Phys. Control. Fusion* **55** 125016 (2013)
[24] H. R. Wilson, et al. *Plasma Phys. Control. Fusion* **48** A71 (2006)